A QUANTITATIVE METHOD TO OPTIMISE MAGNETIC FIELD LINE FITTING OF OBSERVED CORONAL LOOPS

L. CARCEDO[1], D. S. BROWN[1], A. W. HOOD[1], T. NEUKIRCH[1] and T. WIEGELMANN[1,2]

[1] *School of Mathematics and Statistics, University of St. Andrews, St. Andrews, KY16 9SS, U.K. (e-mail: laura@mcs.st-and.ac.uk)*

[2] *Max-Planck-Institut für Aeronomie, Max-Planck-Str. 2, 37191 Katlenburg-Lindau, Germany*

(Received 12 June 2003; accepted 23 September 2003)

Abstract. Many authors use magnetic-field models to extrapolate the field in the solar corona from magnetic data in the photosphere. The accuracy of such extrapolations is usually judged qualitatively by eye, where a less judgemental quantitative approach would be more desirable. In this paper, a robust method for obtaining the best fit between a theoretical magnetic field and intensity observations of coronal loops on the solar disk will be presented. The method will be applied to *Yohkoh* data using a linear force-free field as an illustration. Any other theoretical model for the magnetic field can be used, provided there is enough freedom in the model to optimize the fit.

1. Introduction

Since the solar corona is a low-β plasma, its structure and dynamics are dominated by the local magnetic field. Eruptive events, such as flares, coronal mass ejections (CMEs) and eruptive prominences are driven by excess energy in the magnetic field. Knowledge of the magnetic structure of the corona plays a key role in providing a more complete understanding of such events.

Present observations of coronal loops can be divided into two classes, namely those observed above the solar disk and those observed above the limb. Although the loops above the solar disk are genuinely three-dimensional structures, their observations in soft X-rays and EUV provide images that are projected onto the disk and so only provide two-dimensional information. Essentially, detailed information about the height is lost. These restrictions will be removed by the NASA's Solar Terrestrial Relations Observatory (STEREO) mission, which will use two identically equipped spacecraft to provide 3-D imaging of the Sun. However, until that time, two-dimensional information is all that is available. Aschwanden *et al.* (1999) have developed a method of dynamic stereoscopy to reconstruct the three-dimensional geometry of loops, where the solar rotation is used to vary the aspect angle of otherwise static structures. This method assumes that the loops do not change significantly in time.

Solar magnetographs use the polarization of spectral lines to measure the magnetic field in the photosphere. At the moment, there is no useful method for meas-

Solar Physics **218:** 29–40, 2003.

uring the magnetic field in the corona. In principle, the polarization of emissions from magnetic-sensitive coronal-line transitions can be used to draw conclusions about the coronal magnetic field. These lines, however, are very faint so that in the past they have only occasionally been used (e.g., House, 1977; Arnaud and Newkirk, 1987).

To complement this, the new topic of coronal seismology can provide some information about the coronal magnetic field based on a detailed knowledge of the MHD waves modes (e.g., Roberts, Edwin, and Benz, 1984; Nakariakov and Ofman, 2001; De Moortel and Hood, 2000).

As the coronal field is largely unknown, the only method to deduce the magnetic structure of the corona is to extrapolate it using theoretical models from magnetic field data in the photosphere.

One class of theoretical models are force-free fields. These have the assumptions discussed below.

(1) The coronal magnetic field, **B**, may depend on one or more parameters. For example, in the corona, the *force-free* assumption

$$\mathbf{j} \times \mathbf{B} = \mathbf{0} \tag{1}$$

is justified if the plasma β is small (for a different point of view see Gary, 2001). So, the field can be described by

$$\nabla \times \mathbf{B} = \alpha \mathbf{B}. \tag{2}$$

– $\alpha = 0$ corresponds to the potential case (e.g., Schmidt, 1964; Semel, 1967; Sakurai, 1982; Rudenko, 2001).

– $\alpha = constant$ provides the linear, force-free case (e.g., Nakagawa and Raadu, 1972; Chiu and Hilton, 1977; Seehafer, 1978, 1982; Alissandrakis, 1981; Semel, 1988; Gary, 1989; Lothian and Browning, 1995).

– If α varies with the position, then the resulting magnetic field is a non-linear, force-free field (e.g., Sakurai, 1981; Amari *et al.*, 1997; McClymont, Jiao, and Mikic, 1997; Wheatland, Sturrock, and Roumeliotis, 2000).

(2) Magnetograms of the area can provide a boundary condition for the magnetic field in the photosphere.

(3) Because of the small value of magnetic resistivity (or equivalently, the large value of the magnetic Reynolds number, R_m), the magnetic field and the plasma are 'frozen-in' together. The negligible perpendicular thermal conduction means that heat rapidly spreads along the field but cannot diffuse across the field. Thus, neighboring field lines can have a very different temperature. Hence, it is thought that the enhanced intensity outlines the local magnetic field in coronal loops (e.g., Zirin, 1971; Frazier, 1972; Poletto *et al.*, 1975; Levine, 1976).

Magnetic extrapolation has been used in many other studies. For example, Tang *et al.* (2000) studied a brightening event that occurred on 18 May 1994. They used *Yohkoh* soft X-ray images, vector magnetograms and Hα filtergrams and produced

a magnetic extrapolation using a linear force-free field. The fit to the observations was produced by trial and error.

Van Driel-Gesztelyi *et al.* (2000) studied two sigmoid events (on 25 October 1994 and 14 October 1995) and both were related to the onset of CMEs. Stokes vector magnetograms, from Mees Observatory, were matched to *Yohkoh* soft X-ray images using a linear force-free field. The method of construction is not specified.

Régnier and Amari (2001) and Régnier, Amari, and Kersalé (2002) studied the active region NOAA 8151 (11–13 February 1998) in which a filament eruption is linked to the disappearance of a sigmoidal structure. Observational data was taken from *Yohkoh* soft X-ray images and vector magnetograms (from Mees Observatory) and a nonlinear force-free field using a vector potential, Grad–Rubin-like method (Amari, Boulmezaoud, Mikic, 1999) was calculated numerically.

In order to fit the loops observed with extrapolated field lines, it is necessary to find the best value of the parameters that define the magnetic field (for example, α in the linear force-free case). To do that, the usual method is: choose a value of the parameters, plot some field lines and compare them with the shape of the observed loops. If they do not look similar, another value for the parameters is chosen until a 'similar' shape is found.

In this paper the efficiency of this method is questioned. What makes one fit better than another? In some cases, a slight change of the parameters does not change the field line profile significantly, so no firm conclusions can be drawn about which is the best approximation. Also, fitting a two-dimensional image to a 3D magnetic field calculation introduces an additional free parameter that has to be determined, namely the height of the field lines.

For these reasons, it is necessary to produce a more quantitative than a qualitative method to measure just how accurate the magnetic field extrapolation is. A possible approach to this problem is presented in this paper. Section 2 describes the general method and Section 3 illustrates its use for the particular case of a linear force-free field (although the method can be used by any model that describes the magnetic field using a set of parameters).

Some effort in this direction has been introduced by Wiegelmann and Neukirch (2002). They present a similar method but for three-dimensional structures, that will be applied to data from the SECCHI instrument aboard the STEREO mission.

2. Method of Approach

The method is split into several steps and a more detailed description of each step will be presented in Section 3 in the form of an example. While certain parts of the procedure can be automated, there are other sections that do require human intervention.

(1) Align the magnetic data (e.g., from SOHO/MDI) and the loop image (e.g., X-ray from *Yohkoh*/SXT, or EUV from SOHO/EIT or TRACE, or Hα from the

Solar Flare Telescope at the NAOJ): in general, photospheric magnetograms and loop images are taken from different instruments and not necessarily at the same time. For these reasons it is necessary to align both observations so that they are looking at the same area. Standard solar-software IDL routines can be used for this purpose.

(2) Identify the loop and its foot-point areas: the loop is identified in the intensity image and care should be taken to select a loop that does not have any other loops crossing either in front or behind it. In addition, it is essential that, to some degree, the complete loop can be seen. The footpoints are taken as the ends of the loop in the intensity, unless there is a dominant polarity source seen in the magnetograms. For simplicity, each foot-point area is a circle defined by its center and radius, although a more complex definition could be applied. The value of the center and radius is chosen so the entire end of the loop is included on it (or the entire source in the magnetogram).

(3) Select a value for the magnetic-field parameter, α: at this stage, α is simply an adjustable parameter or set of parameters in the magnetic-field model. For the force-free assumption, α describes the non-potential nature of the field. In general though, α can be a (many) parameter(s) in the magnetic-field model and the method is not restricted to force-free fields.

(4) Calculate a set of field lines: the starting points for the field-line calculations are spread over both footpoint areas. Each field-line equation is integrated, from a starting point inside one of the footpoint areas, until the field line either returns to the photosphere or leaves the region of interest. If the ends of the field line lie inside both footpoint areas, it is accepted, otherwise it is rejected. Thus, only the field lines that go from one footpoint area to the other will be used. However, while the end points may be correct, the shape of the field lines may be entirely different from the shape of the loop. A method to describe how well a field line fits the observed loop must be determined.

(5) For each field line, calculate the deviation between the field line and the intensity pattern, $C_i(\alpha)$: a two-dimensional coordinate system is chosen that uses the distance along the field line as one of the coordinates and the distance perpendicular to the field line as the other. In this manner the field line is 'uncurled' or straightened out. The effect is to give, at each location, j, along the loop, an intensity variation perpendicular to the field, $I_j(N)$, where N is the perpendicular normal coordinate. This intensity profile is fitted by a Gaussian and the maximum of the Gaussian is taken as the location of the loop. This will occur at $N = N_{\max,j}$. If $N_{\max,j} = 0$, then the loop and the field line are at the same location. In general, $N_{\max,j} \neq 0$ so that there is a discrepancy between the loop location and the field line. The standard deviation, $C_i(\alpha)$, of this difference is calculated. For the ith field line this is given by

$$C_i^2(\alpha) = \sum_{j=1}^{M} \frac{N_{\max,j}^2}{(M-1)}, \tag{2}$$

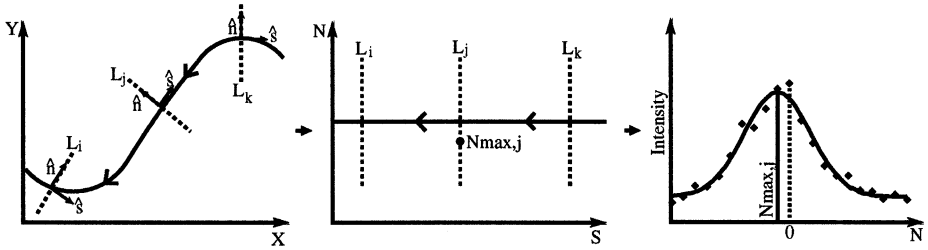

Figure 1. The unit vectors $\hat{\mathrm{s}}$ and $\hat{\mathrm{n}}$, representing unit vectors parallel and perpendicular to the direction of the field line, define the coordinate system for the straightened-out field line. The lines L_i, L_j and L_k are normal to the field line at locations s_i, s_j and s_k along the field line. The intensity along L_j, i.e., across the field line, is shown.

where M is the number of locations along the S coordinate. The method is illustrated in Figure 1.

(6) Calculate the overall deviation for the chosen value of α, $C(\alpha)$: the value of $C_i(\alpha)$ will vary from field line to field line. These deviations must be combined to give a measure $C(\alpha)$ for a specific value of α. In this paper, both the average and the minimum values of $C_i(\alpha)$ will be calculated and compared. However, more complex strategies could be used instead.

(7) Repeat the procedure for different values of α. The value of α that gives the overall global minimum of C provides the best fit to that particular observed loop.

3. Application to Linear Force-Free Coronal Loops

3.1. Coronal magnetic field

The procedure is illustrated using an example to fit linear force-free fields to *Yohkoh*/SXT images of coronal loops. In this case the parameter α is the linear force-free constant determining the amount of non-potential current in the system.

It is likely that the actual coronal magnetic field will not be a linear force-free field, but this provides a simple illustration of the proposed field line fitting method.

For the *linear force-free field* case, the problem is to solve in the upper half-space $\{z \geq 0\}$

$$\nabla \times \mathbf{B} = \alpha \mathbf{B}, \tag{3}$$

$$\nabla \cdot \mathbf{B} = 0, \tag{4}$$

using the magnetogram data from MDI to specify the line-of-sight magnetic field component at the photospheric boundary.

Assuming that the region of study is near the disk center, and ignoring the photosphere curvature, a Cartesian system of coordinates is used. In this system, z refers to the height and (x, y) to the photospheric plane at $z = 0$. A magnetogram

will give the B_z component at $z = 0$. If the field vanishes at large height, the boundary conditions can be expressed as

$$B_z(x, y, 0) = B_0(x, y), \tag{5}$$

$$\lim_{z\to\infty} \mathbf{B}(x, y, z) = 0. \tag{6}$$

There are several ways of solving these equations to obtain the spatial variation of **B**:

(1) In terms of Bessel functions (Schatzman, 1961).

(2) In terms of Fourier series (Nakagawa and Raadu, 1972).

(3) In terms of Green's functions (Chiu and Hilton, 1977).

The method chosen in this work is the third one for which the most general solution is

$$\begin{aligned}\mathbf{B}(x, y, z) = {} & \frac{1}{2\pi} \int_{-\infty}^{\infty}\int_{-\infty}^{\infty} \mathbf{G}(x - x', y - y', z) B_z(x', y', 0)\, \mathrm{d}x'\, \mathrm{d}y' + \\ & + \frac{1}{2\pi} \int_{-\infty}^{\infty}\int_{-\infty}^{\infty} \tilde{\mathbf{G}}(x - x', y - y', z) C(x', y')\, \mathrm{d}x'\, \mathrm{d}y'.\end{aligned} \tag{7}$$

Here $C(x, y)$ is an arbitrary function of the source coordinates, **G** is the Green's function and $\tilde{\mathbf{G}}$ is the 'complementary' Green's function necessary to make Equation (7) a general solution for the magnetic field. The Green's function components G_x, G_y and G_z are of the form:

$$\begin{aligned} G_x(x, y, z, x', y') &= \frac{x - x'}{R}\frac{\partial\Gamma}{\partial z} + \alpha\Gamma\frac{y - y'}{R}, \\ G_y(x, y, z, x', y') &= \frac{y - y'}{R}\frac{\partial\Gamma}{\partial z} - \alpha\Gamma\frac{x - x'}{R}, \\ G_z(x, y, z, x', y') &= -\frac{\Gamma}{R} - \frac{\partial\Gamma}{\partial R}, \end{aligned} \tag{8}$$

where

$$\Gamma = \frac{z\cos(\alpha\rho)}{R\rho} - \frac{\cos(\alpha z)}{R}. \tag{9}$$

Meanwhile, $\tilde{\mathbf{G}}$ has the same structure as **G** with Γ replaced by a function $\tilde{\Gamma}$ whose expression is

$$\tilde{\Gamma} = \frac{z\sin(\alpha\rho)}{R\rho} - \frac{\sin(\alpha z)}{R}. \tag{10}$$

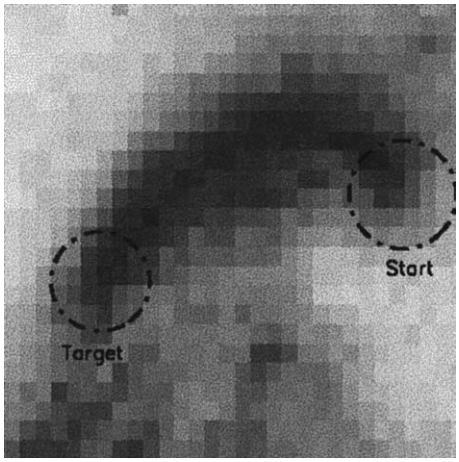

Figure 2. Yohkoh image of a coronal loop. The two footpoint areas are indicated by the *dashed circles*. The *start* area is where the starting points of the field lines are localised. Field lines that do not reach the *target* area are discarded.

For any given value of α, the boundary data for $B_z(x, y, 0)$ fix the contribution to the field from $\mathbf{G}$, but $\tilde{\mathbf{G}}$ is a homogeneous solution whose contribution to the field is not determined by the boundary conditions, except for the potential case ($\alpha = 0$), when $\tilde{\Gamma} = 0$.

For the purpose of this study, $C(x, y)$ is set equal to zero everywhere, since varying the choice of α gives sufficient freedom to obtain a qualitative match to the real field. This choice is often made in the literature (e.g., Lothian and Browning, 1995), and it is equivalent to setting $\partial B_z/\partial z = 0$ everywhere on the boundary except at the sources of $\mathbf{B}$, where it is fixed by the strength of the source.

Petrie and Lothian (2003) studied the effect of including the complementary Green's function. Choosing $C(x, y) = bB_z(x, y)$, where b is a real parameter, some simple systems where studied. They concluded that, the effect of b depends on the topological stability of the system and is less straightforward than the familiar response to varying α.

3.2. Example of method using a *Yohkoh* loop

The data used in this example corresponds to an active region studied by Glover *et al.* (2001) during three consecutive rotations. During the first and the second rotations (March and April 2000), it dominated activity on the disk. During its third rotation two CMEs took place. This study has been done prior to the first CME during the third rotation.

Figure 2 shows a coronal loop observed in SXT; the footpoint areas are indicated in the figure and the starting footpoint area is chosen as the right-hand one. Therefore, the target footpoint area is the left hand one. Starting points for the field line integration are chosen inside the starting footpoint area.

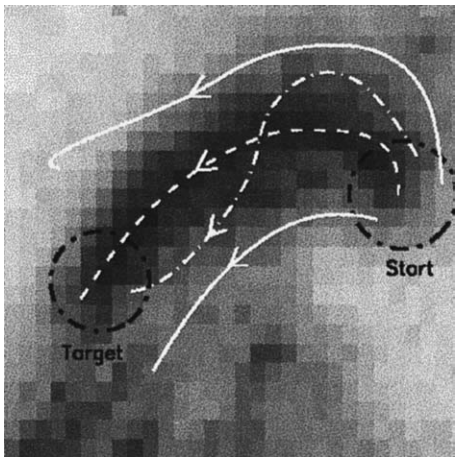

Figure 3. Four simulated field lines starting at the starting footpoint area are shown. There are clearly acceptable field lines (*dashed*) and unacceptable field lines (*solid*) shown.

To illustrate how the proposed method works, Figure 3 shows the projection of some simulated field lines onto the *Yohkoh* image. The acceptable field lines (dashed curves) end in the target footpoint area but there are also several field lines that are unacceptable (solid curves) since they do not reach the target area. Of the two acceptable field lines, one looks like a better fit than the other. It is the object of this paper to determine the quality of the field line fit. A measure of how well the field line fits the observations is now discussed.

Each of the acceptable field lines is 'straightened' out along the corresponding SXT image (Figure 4), and a measure of the deviation, C, between the field line and the image is calculated. In this example, 330 field lines (acceptable and unacceptable) were calculated for each value of α; their starting points were spread evenly through both footpoint areas. For the field line shown in Figure 4 the value of C is 4.26 Mm, while the value of α is 0.016 Mm^{-1}.

Finally, the value of α that provides the best fit is estimated. Figure 5 shows $C(\alpha)$, for $\alpha \in [5, 25] \times 10^{-3}$ Mm^{-1}, plotting both the average and the minimum of C for all acceptable field lines. For α less than 8.74×10^{-3} Mm^{-1} and greater than 21.15×10^{-3} Mm^{-1}, there are no field lines that finished in the target area. Note that the variation of C is similar when considering either the minimum or the average of all the field lines. The result for α is 0.016 ± 0.001 Mm^{-1}. For such an α, $C_{\mathrm{min}} \approx 2.80$ Mm and $C_{\mathrm{avr}} \approx 8.35$ Mm.

4. Discussion and Conclusions

This paper has presented a simple technique for optimizing the fit of a theoretical coronal magnetic field model to X-ray (or other coronal) observations. The method

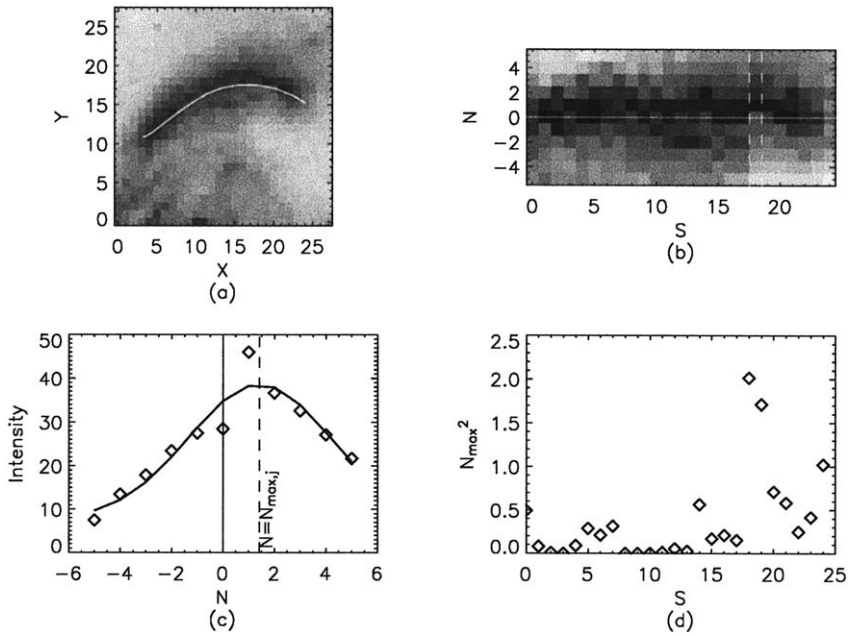

Figure 4. (a) The original SXT image and a superimposed acceptable field line. (b) The 'uncurled' field line and the transformed SXT image. (c) The transverse intensity profile and Gaussian fit at a chord located at $S = 18$, as shown in (b). (d) The difference between the field line and the intensity as a function of the distance along the loop. All the lengths on these plots (such as X, Y, S, and N) are specified in pixels of the SXT image. Each pixel has a width of 7.13 Mm.

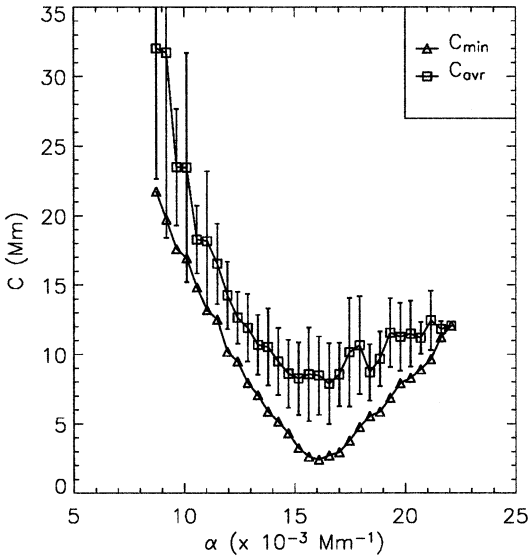

Figure 5. The variation of C with the value of α, showing both, the average ($C_{\rm avr}$) and the minimum ($C_{\rm min}$) values for all field lines. The error of $C_{\rm avr}$ is calculated as the mean absolute deviation.

provides a set procedure for fitting the magnetic field in an objective manner, removing the subjective nature of previous methods that simply pick field lines that are similar in shape to an observed coronal loop. Here a collection of magnetic field lines are fitted by minimizing the deviation between them and the intensity pattern, rather than just picking one field line and fitting it by eye.

There are seven steps in the procedure and these are described in Section 2. Step one consists of a proper alignment between magnetograms and coronal images.

The user has important decisions to make in step two. Here the end points of the coronal loop are identified by eye, from either the ends of the coronal emission or from dominant polarity sources in magnetograms. These footpoints are individually modeled by circles, whose center and radii must be given.

The remaining steps are essentially automated. The accuracy of α depends on its range and step size ($\delta\alpha$), bearing in mind that some values of α may produce no acceptable field lines.

The calculation of the field lines in step four, starting from the one of the photospheric footpoints, depends on the particular theoretical model being used. However, enough field lines must be calculated to be representative of the flux connectivity of the footpoints. Although the fitting procedure applies to any theoretical magnetic field model, the constant α solution is used here. It is determined as an analytical expression in terms of a Green's function solution.

Step five is the key to the field-line fitting technique. A particular acceptable field line is selected and a coordinate system based on the distance along and perpendicular to this field line is constructed. The coronal image is then transformed into this coordinate system and the position of the coronal loop, in terms of the maximum of the coronal emission, is deduced. The position of the coronal loop is obtained by fitting a Gaussian curve to the coronal intensity. The square of the perpendicular distance, N^2, gives a measure of the disparity of the fit at a particular distance along the loop. The total deviation, $C_i(\alpha)$, for this particular field line is calculated by summing the differences at each location. This is repeated for all the other acceptable field lines.

In step six, either the average of C over the acceptable field lines or the minimum C is selected for each value of α.

Finally, step seven repeats the above for different values of α and the best fit is given by the value of α that provides the global minimum C.

The method has been illustrated by using the example of a constant α, linear force-free field. The only free parameter in this case is α and it is adjusted to minimize the standard deviation between the observed and calculated field lines. It is accepted that the constant α field is unlikely to be the correct model for the coronal magnetic field. However, the particular magnetic-field model is not crucial to demonstrate the feasibility of the fitting technique described in this paper.

This method is easily extendable to magnetic-field models with multiple parameters, though the time taken to scan multidimensional parameter space will increase exponentially with the number of parameters. One example could be to

take the complementary part of the linear force-free field into account (Petrie and Lothian, 2003). Another possibility would be to use the method of Petrie and Neukirch (2000) with a wider class of MHS solutions depending on additional parameters.

In future, this method will be applied to more general magnetic field models. To show the advantages of this fitting approach, other data sets will be studied. In particular, it will be useful to study the same active region over a period of time. The constant α field can be used to investigate how the value of α changes before and after the eruption of a coronal mass ejection.

In this paper *Yohkoh*/SXT data has been used to judge the quality of the extrapolated field lines for different values of the field parameters. It should be noted that observations of the same region with different wavelength filters will outline plasma at different temperatures. It would be interesting to see whether the different observations of the same region are indeed represented by a common α in a linear force-free model, or whether the value of α varies significantly. This would provide a measure of the quality of the linear force-free model in a localised region of the corona, and would have implications on the validity of using this model to study changes in α over a period of time.

Acknowledgements

L. Carcedo, D. S. Brown, and T. Neukirch thank PPARC for financial support. T. Wiegelmann has been supported by an EC Marie-Curie Fellowship and by the DLR grant 500C0007.

References

Alissandrakis, C. E.: 1981, *Astron. Astrophys.* **100**, 197.
Amari, T., Boulmezaoud, T. Z., and Mikic, Z.: 1999, *Astron. Astrophys.* **350**, 1051.
Amari, T., Aly, J. J., Luciani, J. F., Boulmezaoud, T. Z., and Mikic, Z.: 1997, *Solar Phys.* **174**, 129.
Arnaud, J. and Newkirk, G.: 1987, *Astron. Astrophys.* **178**, 263.
Aschwanden, M. J., Newmark, J. S., Delaboudinière, J.-P., Neupert, W. M., Klimchuk, J. A., Gary, G. A., Portier-Fozzani, F., and Zucker, A.: 1999, *Astrophys. J.* **515**, 842.
Chiu, Y. T. and Hilton, H. H.: 1977, *Astrophys. J.* **212**, 873.
De Moortel, I. and Hood, A. W.: 2000, *Astron. Astrophys.* **363**, 269.
Frazier, E. N.: 1972, *Solar Phys.* **24**, 98.
Gary, G. A.: 1989, *Astrophys. J. Suppl. Ser.* **69**, 323.
Gary, G. A.: 2001, *Solar Phys.* **203**, 71.
Glover, A., Harra, L. K., Matthews, S. A., Hori, K., and Culhane, J. L.: 2001, *Astron. Astrophys.* **378**, 239.
House, L. L.: 1977, *Astrophys. J.* **214**, 632.
Levine, R. H.: 1976, *Solar Phys.* **46**, 159.
Lothian, R. M. and Browning, P. K.: 1995, *Solar Phys.* **161**, 289.
McClymont, A. N., Jiao, L., and Mikic, Z.: 1997, *Solar Phys.* **174**, 191.

Nakagawa, Y. and Raadu, M. A.: 1972, *Solar Phys.* **25**, 127.
Nakariakov, V. M. and Ofman, L.: 2001, *Astron. Astrophys.* **372**, L53.
Petrie, G. J. D. and Lothian, R. M.: 2003, *Astron. Astrophys.* **398**, 287.
Petrie, G. J. D. and Neukirch, T.: 2000, *Astron. Astrophys.* **356**, 735.
Poletto, G., Vaiana, G. S., Zombeck, M. V., Krieger, A. S., and Timothy, A. F.: 1975, *Solar Phys.* **44**, 83.
Régnier, S. and Amari, T.: 2001, in P. Brekke, B. Fleck, and J. B. Gurman (eds.), *Recent Insights into the Physics of the Sun and Heliosphere: Highlights from SOHO and other Space Missions*, Astronomical Society of the Pacific, San Francisco, p. 441.
Régnier, S., Amari, T. and Kersalé, E.: 2002, *Astron. Astrophys.* **392**, 1119.
Roberts, B., Edwin, P. M., and Benz, A. O.: 1984, *Astrophys. J.* **279**, 857.
Rudenko, G. V.: 2001, *Solar Phys.* **198**, 5.
Sakurai, T.: 1981, *Solar Phys.* **69**, 343.
Sakurai, T.: 1982, *Solar Phys.* **76**, 301.
Schatzman, E.: 1961, *Ann. d'Astrophys.* **24**, 251.
Schmidt, H. U.: 1964, in W. N. Ness (ed.), *ASS-NASA Symposium on the Physics of Solar Flares*, p. 107.
Seehafer, N.: 1978, *Solar Phys.* **58**, 215.
Seehafer, N.: 1982, *Solar Phys.* **81**, 69.
Semel, M.: 1967, *Ann. d'Astrophys.* **30**, 513.
Semel, M.: 1988, *Astron. Astrophys.* **198**, 293.
Tang, Y. H., Li, Y. N., Fang, C., Aulanier, G., Schmieder, B., Démoulin, P., and Sakurai, T.: 2000, *Astrophys. J.* **534**, 482.
van Driel-Gesztelyi, L. *et al.*: 2000, *J. Atmospheric Solar-Terrest. Phys.* **62**, 1437.
Wheatland, M. S., Sturrock, P. A., and Roumeliotis, G.: 2000, *Astrophys. J.* **540**, 1150.
Wiegelmann, T. and Neukirch, T.: 2002, *Solar Phys.* **208**, 233.
Zirin, H.: 1971, in R. Howard (ed.), 'Solar Magnetic Fields', *IAU Symp.* **43**, 237.